Research Paper

GEOSPHERE

GEOSPHERE, v. 16

https://doi.org/10.1130/GES01692.1

9 figures; 1 set of supplemental files

CORRESPONDENCE: rodrigueze@email.arizona.edu

CITATION: Rodriguez, E.E., and Russo, R.M., 2019, Southern Chile crustal structure from teleseismic receiver functions: Responses to ridge subduction and terrane assembly of Patagonia: Geosphere, v. 16, https://doi.org/10.1130/GES01692.1.

Science Editor: Shanaka de Silva
Associate Editor: Craig H. Jones

Received 13 March 2018
Revision received 30 July 2019
Accepted 17 October 2019

Southern Chile crustal structure from teleseismic receiver functions: Responses to ridge subduction and terrane assembly of Patagonia

E.E. Rodriguez* and R.M. Russo

Department of Geological Sciences, University of Florida, Gainesville, Florida 32611, USA

ABSTRACT

Continental crustal structure is the product of those processes that operate typically during a long tectonic history. For the Patagonia composite terrane, these tectonic processes include its early Paleozoic accretion to the South America portion of Gondwana, Triassic rifting of Gondwana, and overriding of Pacific Basin oceanic lithosphere since the Mesozoic. To assess the crustal structure and glean insight into how these tectonic processes affected Patagonia, we combined data from two temporary seismic networks situated inboard of the Chile triple junction, with a combined total of 80 broadband seismic stations. Events suitable for analysis yielded 995 teleseismic receiver functions. We estimated crustal thicknesses using two methods, the *H-k* stacking method and common conversion point stacking. Crustal thicknesses vary between 30 and 55 km. The South American Moho lies at 28–35 km depth in forearc regions that have experienced ridge subduction, in contrast to crustal thicknesses ranging from 34 to 55 km beneath regions north of the Chile triple junction. Inboard, the prevailing Moho depth of ~35 km shallows to ~30 km along an E-W trend between 46.5°S and 47°S; we relate this structure to Paleozoic thrust emplacement of the Proterozoic Deseado Massif terrane above the thicker crust of the North Patagonian/Somún Cura terrane along a major south-dipping fault.

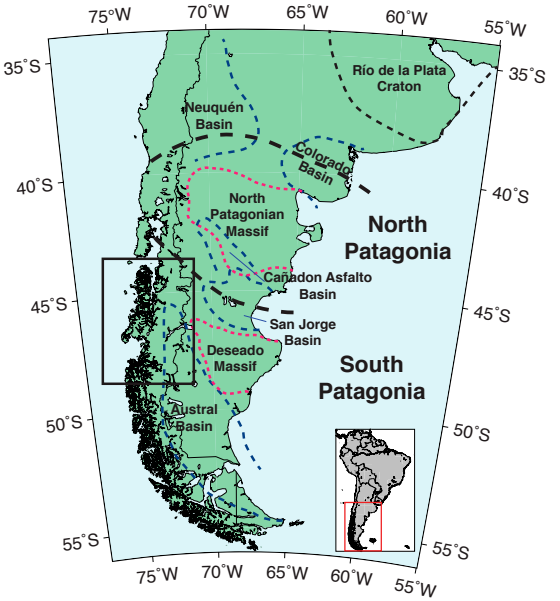

Figure 1. Map of Patagonia basement terranes. Massifs are differentiated by red dashed borders, basins are shown in dashed blue, and the Rio de la Plata is denoted by a black dashed line. Heavy dashed black line shows approximate limits of North and South Patagonia lithosphere. Study area limits are shown by black rectangle. Figure is modified from Ramos (2008), Rapela et al. (2007), and Pankhurst et al. (2006).

INTRODUCTION

Tectonic History

Southernmost South America (Fig. 1), comprising continental terranes south of the Río de la Plata craton (Rapela et al., 2007; Ramos, 2008), has been perhaps the least studied of continental regions—at least using seismic techniques. Patagonia is an unusually young continental mass, due to its relatively recent (Paleozoic) amalgamation, which brought together continental fragments formed through magmatic processes during several episodes in the Proterozoic (e.g., Mundl et al., 2015, 2016; Schilling et al., 2017). Noteworthy tectonic processes that affected these Patagonian terranes include Carboniferous–Permian accretion of the North Patagonia or Somún Cura Massif and the Deseado Massif, and, possibly a distinct South Patagonia terrane, to form the composite Patagonia terrane (Fig. 1), and its accretion to the South American portion of Gondwana (e.g., Schilling et al., 2017). Subsequent Mesozoic rifting of South America from Africa formed the wide South Atlantic passive margin and the Austral Magallanes Basin (e.g., Varela et al., 2012). Finally, a long history of subduction of oceanic lithosphere beneath western Patagonia began in the Mesozoic, and this has included episodes of spreading ridge subduction (e.g., Cande and Leslie, 1986; Breitsprecher and Thorkelson, 2009) and attendant volcanism during the late Cenozoic (e.g., Ramos, 1989; Gorring et al., 1997; Gorring and Kay, 2001). In this study, we focused on two aspects of this tectonic history by examining crustal structures related to the assembly of Patagonia from disparate continental fragments, and structural variability due to subduction of spreading segments of the Chile Ridge.

*Now at Department of Geosciences, University of Arizona, Tucson, Arizona 85721, USA.

The collisional assembly and later extensional history of Patagonia are recorded in the extant deformation of its basement terranes, two northwest-trending massifs, and bordering basins (Fig. 1). The North Patagonia Somún Cura Massif was deformed during the collision of North Patagonia with Gondwana and is bounded by the Cañadón Asfalto Basin to the south. The Deseado Massif was affected by the collision of southern Patagonia with northern Patagonia during the Carboniferous, as recorded by regional metamorphism (Pankhurst et al., 2006; Ramos, 2008). The Deseado Massif is bounded by the San Jorge Basin to the north and the Austral Magallanes Basin to the south, which opened in the Jurassic during a period of widespread extension (Wilson, 1991; Varela et al., 2012). The boundaries between the basement massifs and the basins are not well defined, spatially, due to limited outcrop and an almost complete lack of observable contacts between identifiable units within either the massifs or basins (Ramos, 2008). It is unclear based on geologic observations, for example, whether or not the crust underlying the Austral Basin is identical to or differs in some way from that of the adjacent Deseado Massif.

Currently, the tectonic activity of Patagonia is largely dominated by the subduction of the Chile Ridge, the active spreading ridge between the Antarctic and Nazca plates, which intersects the Chile Trench, forming a trench-trench-ridge triple junction (Herron et al., 1981). The Chile Ridge began subducting beneath southernmost South America in the mid-Miocene, and the Chile triple junction has since migrated northward to 46.5°S, where an actively spreading segment is currently in the Chile Trench just offshore from the Taitao Peninsula (Fig. 2; Cande and Leslie, 1986; Breitsprecher and Thorkelson, 2009; Bourgois et al., 2016). The triple junction is notably characterized by differing subduction rates on either side of the Chile Ridge, with the Nazca plate subducting at a rate of 6.6 cm/yr and the Antarctic plate subducting at 1.85 cm/yr (Wang et al., 2007).

The subduction of the Chile Ridge system has been associated with variable, diachronously developed structures and magmatism in the overriding South America plate, where important differences in morphology and structures are found in forearc areas north and south of the present Chile triple junction related to the presence of a slab window (e.g., Ramos, 1989; Gorring et al., 1997; Gorring and Kay, 2001; Russo et al., 2010a, 2010b). The direct effect of the subduction of the relatively young and buoyant oceanic crust produced at the ridge has been hypothesized to yield enhanced subduction erosion and subsequent thinning of the South American crust in areas where the ridge has subducted or is currently subducting. Bourgois et al. (1996) attempted to quantify the volume of this enhanced erosion using geologic and geochemical constraints, in combination with paleoreconstructions, and found a subduction erosion rate of 231–443 $km^3\,km^{-1}\,m.y.^{-1}$, a rate significantly higher than rates of subduction erosion estimated for regions to the north of the Chile triple junction that have not undergone ridge subduction.

In this article, we show that the South American forearc crust is indeed thinned where the Chile Ridge has been subducted, relative to along-strike thicknesses farther north in our study area. We attribute this crustal thinning to enhanced subduction erosion due to ridge subduction (e.g., Bourgois et al., 1996, 2016). We also show that important variations in crustal structure

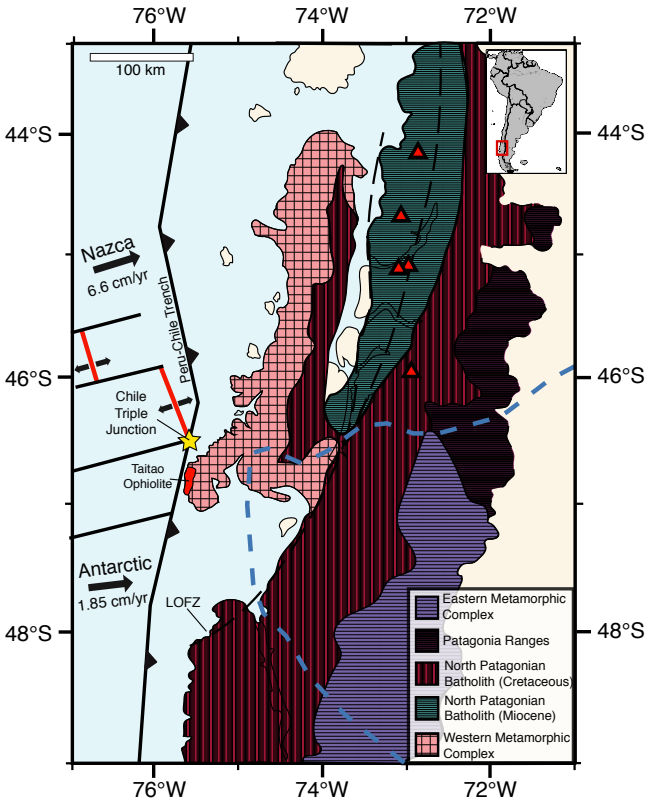

Figure 2. Simplified geologic map of the study region (modified from SERNAGEOMIN, 2003). Volcanoes of the Southern volcanic zone are red triangles. Relative convergence velocities are from Wang et al. (2007). Blue dashed line denotes the edge of the slab window at 50 km depth from Russo et al. (2010a). The black dashed line shows the trace of the Liquiñe-Ofqui fault zone (LOFZ). The study area is delimited by red box in inset, upper right.

appear to have originated during the assembly of Patagonia in the Paleozoic. We resolve a south-dipping, through-going crustal structure that places crust of the Proterozoic Deseado Massif terrane above crust of the North Patagonian–Somún Cura terrane.

Regional Geology

The known basement geology for our study region can be grouped into four distinct units that run approximately parallel to the Nazca–South America subduction zone: Eastern metamorphic complex, Western metamorphic

complex, Patagonian Ranges, and North Patagonian Batholith (Fig. 2). The westernmost part of the study area, including the Guaitecas and Chonos Archipelago islands and Taitao Peninsula, largely consists of surface outcrops of the Western metamorphic complex. In our study area, the Western metamorphic complex is composed of metaturbidite sequences, with some occurrences of metacherts and metabasites, dated to the Mesozoic, with metamorphism likely completed by the Early Jurassic (Hervé and Fanning, 2001).

Bordering the Western metamorphic complex to the east (Fig. 2), the arc domain is composed of the North Patagonian Batholith, a continuous magmatic belt that runs from ~40°S to 53°S. The North Patagonian Batholith is associated with episodic pulses of granitoid intrusions that occurred between the Late Jurassic and Pleistocene (Pankhurst et al., 1999). Two major pulses of North Patagonian Batholith magmatism include Cretaceous and early Miocene bands of felsic intrusions that are nearly identical geochemically (Pankhurst et al., 1999). An early Miocene portion of the North Patagonian Batholith extends northward from the latitude of the Chile triple junction along the active Southern volcanic zone and is divided by the dextral strike-slip Liquiñe-Ofqui fault.

East of the North Patagonian Batholith (Fig. 2), the back-arc domain is divided north-south at ~46.5°S–47°S into two units, the Patagonian Ranges and the Eastern metamorphic complex. The Eastern metamorphic complex is the older of these units, dated to the Late Devonian–early Carboniferous; it outcrops in the southeastern section of our study area (Hervé et al., 2003). The Eastern metamorphic complex is predominantly composed of metaturbidite sequences with some occurrences of higher-grade contact metamorphism near Mesozoic to Cenozoic intrusions (Hervé et al., 2003). The regional metamorphism of the Eastern metamorphic complex likely occurred during the Paleozoic accretion of the Patagonian microplate to South America (Bell and Suárez, 2000).

The Patagonian Ranges, outcropping to the north of the Eastern metamorphic complex, are Middle–Late Jurassic and Late Cretaceous volcanic-sedimentary successions (Pankhurst et al., 1998; Morata et al., 2004; Lagabrielle et al., 2007). A northern, Late Cretaceous group is composed of both intrusive and extrusive rocks ranging from felsic to mafic compositions, including dacitic to basaltic volcanic rocks and intrusive gabbros interbedded with sedimentary deposits (De La Cruz et al., 2003; Morata et al., 2004; Lagabrielle et al., 2007). The Middle–Late Jurassic group to the south is characterized by more felsic volcanic sequences of rhyolitic to dacitic compositions, also interbedded with sedimentary deposits (Pankhurst et al., 1998; Morata et al., 2004; Lagabrielle et al., 2007).

DATA

In order to examine the crustal seismic structure of the region, we used the receiver function method, which relies on observations of the relative traveltimes of the direct P wave to Ps wave. At a subsurface velocity interface of high impedance contrast, for example, the Moho, a P wave will convert some of its energy to an S wave, producing a Ps arrival potentially visible on a radial receiver function. The P wave and Ps converted phase may generate multiple reverberations in the crust, which are also potentially visible on the radial receiver functions (Langston, 1977; Ammon et al., 1990; Ligorria and Ammon, 1999; Zhu and Kanamori, 2000). These converted S waves can be isolated within the P wave coda by deconvolving the vertical component seismogram (including the P wave and its coda) from an equivalent-length time series of the radial component. Iterative deconvolution constructs the time series, called the receiver function, which, when convolved with the vertical component recording, yields the radial component time series (Ligorria and Ammon, 1999), thus isolating the Ps phase and later P to S conversions and reverberations within the crust.

Data were combined from two broadband seismic networks (Fig. 3A), the Chile Ridge Subduction Project (CRSP; data may be obtained from the Incorporated Research Institutions for Seismology [IRIS] Data Management Center, http://ds.iris.edu/ds/nodes/dmc/; https://doi.org/10.7914/SN/YJ_2004), which ran from December 2004 to February 2007, and the Seismic Experiment in the Aisén Region of Chile (SEARCH; data may be obtained from the IRIS Data Management Center, http://ds.iris.edu/ds/nodes/dmc/), which ran from January 2005 to March 2006. The networks included 39 and 41 broadband stations, respectively, yielding a total of 80 stations, and together encompassed an area from ~43.5°S to 48.5°S and 71°W to 76°W. We used a total of 102 earthquakes for the receiver function analysis (Fig. 3B). We used events with magnitudes ≥5.9, from a variety of back azimuths and teleseismic distances (30°–90°). For each event, the north, east, and vertical channels were band-passed using a Butterworth filter with corner frequencies at 0.1–2.0 Hz, and a Gaussian smoothing parameter of 2.5. From these events, 995 receiver functions were produced using the iterative deconvolution method of Ligorria and Ammon (1999). Signal-to-noise was too low at stations QUIT and RIMA of the SEARCH deployment to produce useful receiver functions.

The station distribution of the combined CRSP and SEARCH networks was heterogeneous, particularly in station spacing: Station density was high enough in areas occupied east of 73°W to apply the common conversion point (CCP) stacking technique to the receiver functions, yielding continuous imagery of subsurface structure down to uppermost mantle depths. However, west of 73°W, on the Taitao Peninsula and Chonos and Guaitecas islands, few stations of the SEARCH network were deployed, and those of the CRSP network were spaced at 70–100 km separation, which greatly reduced the quality of CCP imaging. Thus, we had to apply the *H-k* stacking technique to determine crustal structure beneath the western stations of the two deployments.

METHODS AND RESULTS

H-k Stacking Method

Crustal thicknesses, *H*, and compressional to shear wave velocity ratios Vp/Vs, *k*, were calculated using the *H-k* stacking method of Zhu and Kanamori (2000). The *k*-value is directly related to Poisson's ratio and may provide

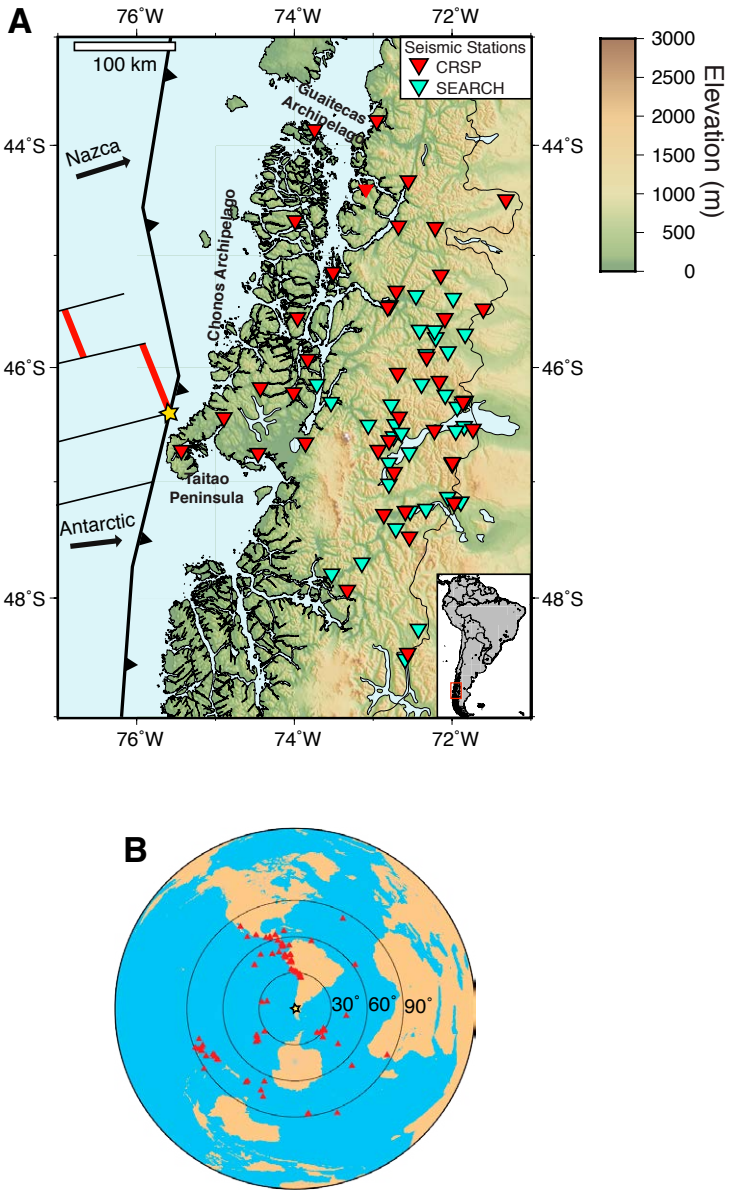

Figure 3. (A) Station map of Chile Ridge Subduction Project (CRSP) and Seismic Experiment in the Aisén Region of Chile (SEARCH) seismic networks. Red inverted triangles are the CRSP network stations, and green inverted triangles are SEARCH network stations. (B) Source events used to construct receiver functions.

information about the crustal composition (e.g., Clarke and Silver, 1993; Zandt and Ammon, 1995; Christensen, 1996). The method entails a two-dimensional grid search for an *H-k* pair that best fits the peaks of the aligned Ps phase and later crustal reverberations of the receiver functions at each station. The method assumes a one-dimensional velocity structure beneath the station for the mantle-crust boundary; however, lateral changes in the velocity structure beneath a station may complicate the grid search, as different ray paths to the station can sample different velocity structures.

We allowed for variable weighting of the contributions of converted phase peaks in determining the best-fitting *H-k* pair. Because converted and reverberating phases were more readily identifiable in receiver functions from some stations than in others, we weighted their contributions to the *H-k* grid search differently; Ps phase weights ranged from 0.5 to 0.9, out of a possible total of 1, and weights of the later-arriving PpPs and PsPs + PpSs phases ranged from 0.05 to 0.3. The Moho depth range, *H*, was originally restricted to lie between 20 and 60 km, and *k* values were allowed to range between 1.5 and 2.0. For some stations, these parameter ranges were further reduced to allow us to focus on more geologically reasonable results.

The *H-k* grid search method can yield multiple possible solutions as a result of a trade-off between *H* and *k*, and receiver functions are often equally well fit by bands of *H-k* values (Fig. 4). To assess the stability of the *H-k* estimate, we used bootstrap resampling of the receiver functions (Sandvol et al., 1998), selecting random subsets of receiver functions for each station, and then rerunning the *H-k* grid search for each of 200 resampled data sets. We detail the *H-k* results and corresponding standard deviations from the bootstrap resampling for individual stations in Table S1 (three-letter coded CRSP network) and Table S2 (four-letter coded SEARCH network) and show results of the grid searches for each station that yielded useful results in Figures S9–S16 (see Supplemental Material[1]).

H-k Stacking Results

For stations in the forearc region, crustal thickness increases northward in the Chonos and Guaitecas Archipelago islands, from 28 to 35 km beneath the Taitao Peninsula to values between 34 and 55 km in the northernmost parts of the islands (Fig. 5A). In the active arc region, crustal thicknesses smoothly shallow southward from ~43 km to 34 km.

Inland, the *H-k* grid search results were less consistent, particularly for the easternmost stations situated in the Patagonian Ranges and the Eastern metamorphic complex, where multiple bands of equally credible results appeared. For a group of stations near the Chile-Argentina border, crustal thicknesses from the *H-k* analyses vary between two bands of equally well-fit *H* and *k* values, spanning Moho depths from 33 to 47 km (Fig. 4). By binning the receiver functions by their back azimuths for these stations, north-south, and rerunning the *H-k* grid search for each bin, the results resolved into a single band of *H-k* values. *H* values from receiver functions from southerly back azimuths were

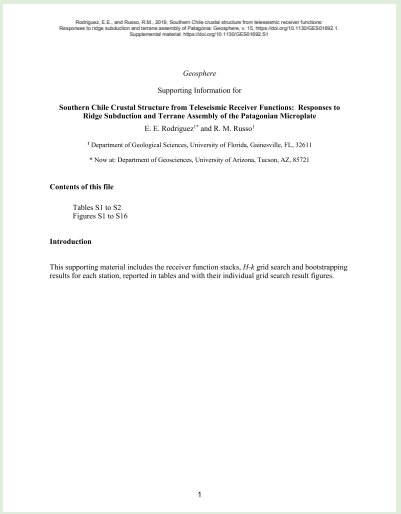

Rodriguez, E.E., and Russo, R.M., 2019, Southern Chile crustal structure from teleseismic receiver functions: Responses to ridge subduction and terrane assembly of Patagonia: Geosphere, v. 15, https://doi.org/10.1130/GES01692.1. Supplemental material: https://doi.org/10.1130/GES01692.S1

Geosphere

Supporting Information for

Southern Chile Crustal Structure from Teleseismic Receiver Functions: Responses to Ridge Subduction and Terrane Assembly of the Patagonian Microplate

E. E. Rodriguez[1*] and R. M. Russo[1]

[1] Department of Geological Sciences, University of Florida, Gainesville, FL, 32611

[*] Now at: Department of Geosciences, University of Arizona, Tucson, AZ, 85721

Contents of this file

Tables S1 to S2
Figures S1 to S16

Introduction

This supporting material includes the receiver function stacks, *H-k* grid search and bootstrapping results for each station, reported in tables and with their individual grid search result figures.

1

[1]Supplemental Material. Includes receiver function stacks, H-k grid search, and bootstrapping results for each station, reported in tables and with their individual grid search result figures. Please visit https://doi.org/10.1130/GES01692.S1 or access the full-text article on www.gsapubs.org to view the Supplemental Material.

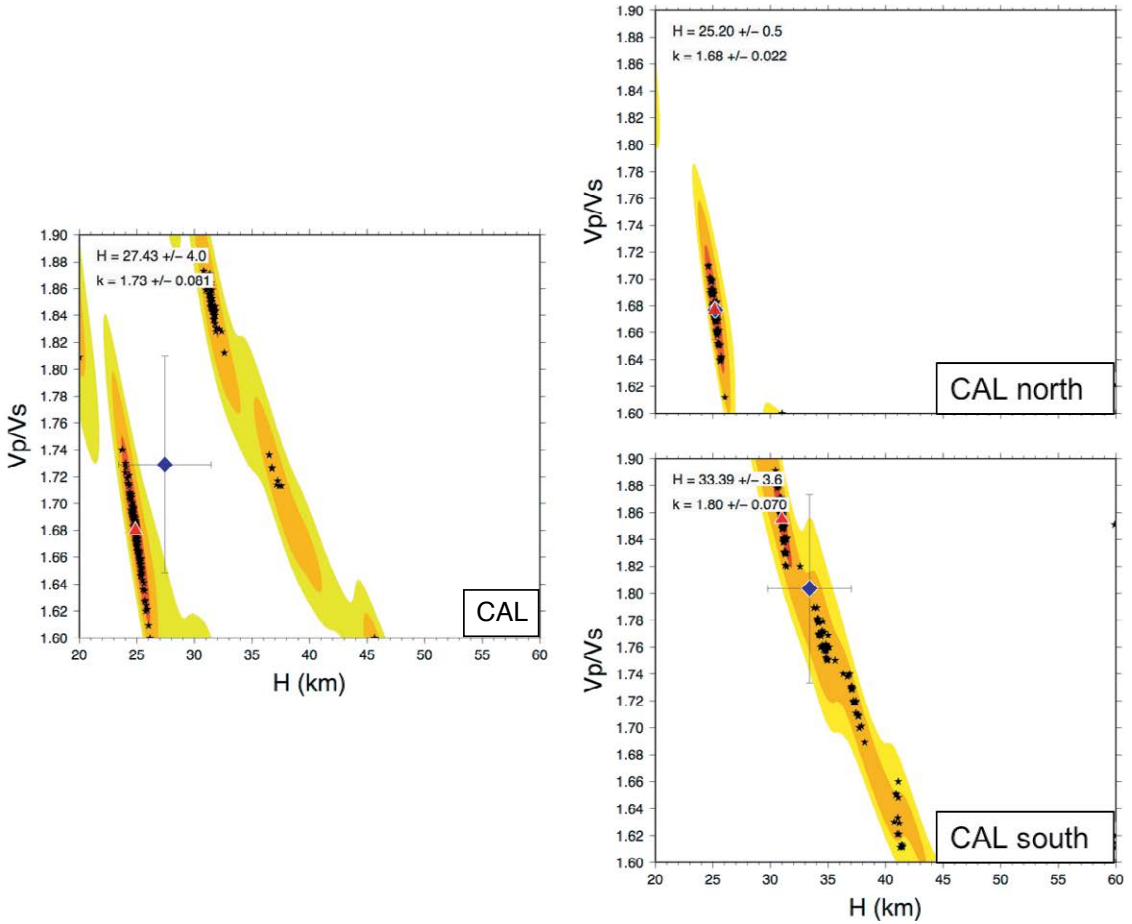

Figure 4. Example multibanded *H-k* grid search from results at station CAL. Left: *H-k* grid search result, all data included. Red triangle—grid search result. Black stars—grid search results for each individual run of the bootstrap. The colored bands show the contours of the grid search, with red being the minimum. Note two bands of *H-k* values fit the receiver functions equally well. Blue diamond is best-fitting *H-k* pair from bootstrapping all data, which is clearly a spurious average of the results for the two bands. Right: Receiver functions divided into two groups: receiver functions from events with northern back azimuths (top), and those from southern back azimuths (bottom). Note the two groups of receiver functions are well fit by two different *H-k* pairs, indicating that the structure beneath this station is highly heterogeneous.

systematically greater (33–47 km) than *H* values from northerly back azimuths (25–33 km). Assuming the best-fitting *H-k* values are valid, the thickest crust in the eastern study area, ranging from 40 to 47 km, occurs beneath the southern, Middle Jurassic Patagonian Range between 45.5°S and 46.5°S. North of 45.5°S, the apparent Moho sharply shallows, within a horizontal distance of less than 50 km, to ~32–35 km. South of 46.5°S, the crust smoothly shallows to ~35 km.

For the forearc region, receiver functions from the three stations of the southern Taitao Peninsula, HOP, NWM, and SAD, yielded *k* values of ~1.64, in contrast to *k* values from Guaitecas and Chonos Archipelago stations, which were ~1.82 (Fig. 5B). To the east, at stations overlying the North Patagonian Batholith, *k* values were intermediate, averaging ~1.70. In the northern Patagonian Ranges, *k* values were ~1.65. South of the northern Patagonian Ranges, in their southern portion and in the Eastern metamorphic complex, where we observed multiple bands of equally likely *H-k* grid search results, the *k* values were much less consistent, ranging between 1.62 and 1.85.

COMMON CONVERSION POINT STACKING METHOD

To improve resolution of the crustal structure of the back-arc region, a second method, the CCP stacking method developed by Dueker and Sheehan (1997), as implemented by Zhu et al. (2006), was employed to reestimate crustal thicknesses in areas where close station spacing could yield reliable imaging. The CCP stacking method involves determining the arriving Ps phase

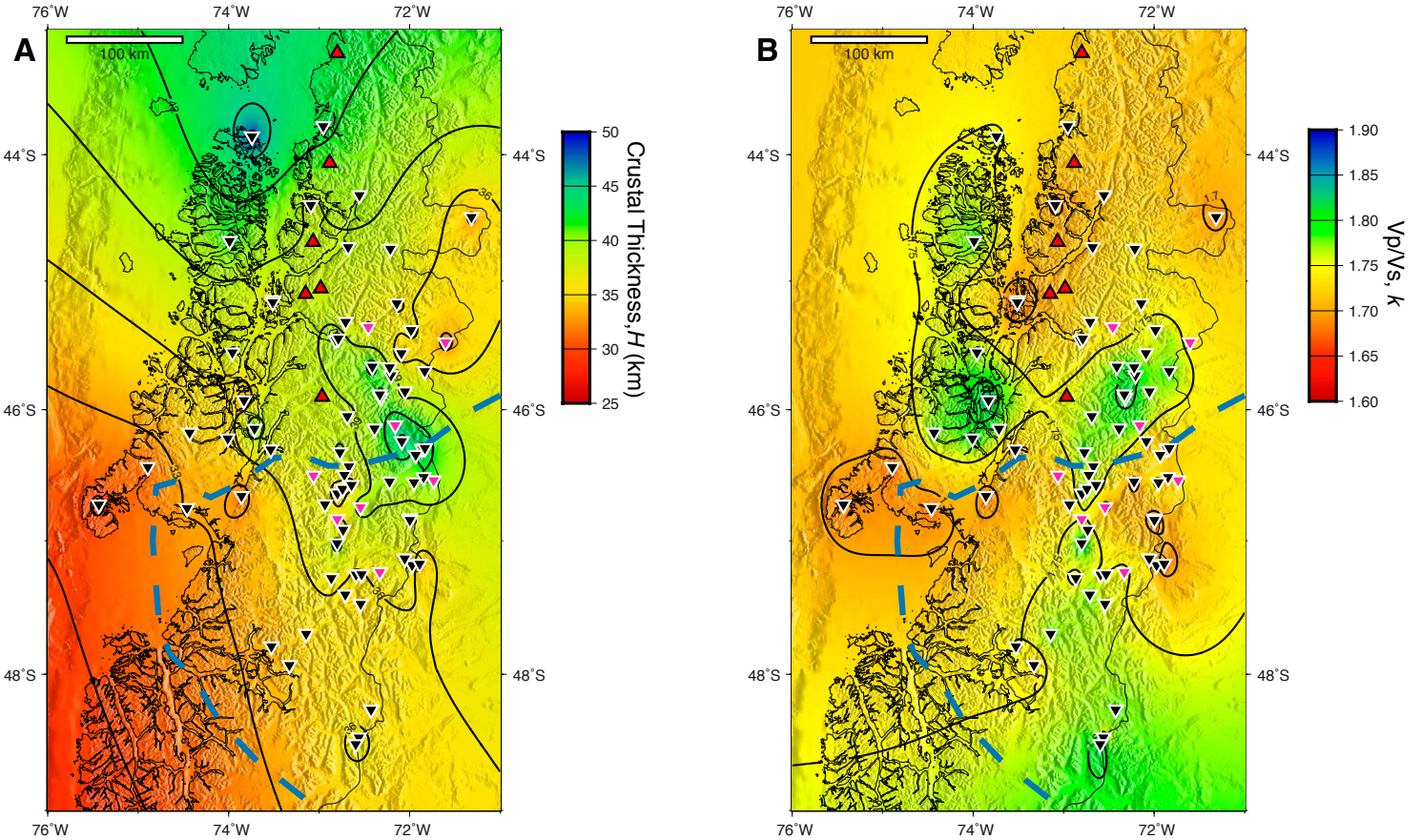

Figure 5. ***H-k*** **stacking bootstrap results. (A) Map of the crustal thickness values,** ***H.*** **Inverted triangles mark stations of the Chile Ridge Subduction Project (CRSP) and Seismic Experiment in the Aisén Region of Chile (SEARCH) networks. Stations that had multiple bands of equally well-fit** ***H-k*** **grid search results are colored pink. (B)** ***H-k*** **stacking results for Vp/Vs values,** ***k.*** **Blue dashed line marks the edge of the slab window at 50 km depth from Russo et al. (2010a).**

ray path from its Moho piercing point up to the station, and also a correction of receiver function amplitudes depending on the angle of incidence of the Ps phase (Dueker and Sheehan, 1997). We used the IASP91 velocity model of Kennett and Engdahl (1991) to migrate the arrival times of P-to-S conversions in the receiver function to depth. We chose to use the IASP91 velocity model rather than our *H-k* results because of the unusually high variability in *k* values in some areas of our study. The use of a one-dimensional (1-D) velocity model introduces variable uncertainties into our depth calculation of conversions, as receiver functions are mainly sensitive to the product of depth and seismic velocity (Ammon et al., 1990); however, modeling by Bishop et al. (2017) has shown that this uncertainty is relatively small, at most ±2.6 km, for a P wave velocity perturbation of 5%. We note also that variation in *k* values from 1.7 to 1.8 entails conversion depth uncertainties of around ±5%. The receiver functions were then binned by their Moho piercing locations—the common conversion point for a group of Ps waves arriving at various stations—and the amplitudes of the receiver functions stacked in each of the bins. Crustal structure could then be determined by taking profiles through the three-dimensional volume (3-D) formed by the composite bins, providing an image of the structure throughout the crust (Fig. 6), rather than at each station, as for the *H-k* stacking method.

CCP Stacking Results

CCP stacking yields a three-dimensional volume of conversion amplitudes, from which cross sections can be extracted. These sections were chosen to pass through regions of highest station density, as they offer the highest resolution as well as the minimum of spuriously interpolated interstation structure. The sections were therefore limited to the eastern (predominantly on-land) section of our study area. For the resulting CCP cross sections, we interpreted the Moho as the continuous, positive-amplitude P-to-S converter between 25 and 45 km depth.

The CCP stacking results reveal an overall northward-thickening crust from 32 to 33 km at the southern margin of our study region at ~47.6°S to 37–38 km at the northern margin at ~45.0°S (Fig. 7). At 47.0°S, the smoothly varying Moho shallows sharply from 35 to 30 km. Northward, the Moho depth remains constant to 46.5°S, where it again deepens to 35 km, deepening further to 37–38 km at 45.0°S. North of ~45.0°S, station spacing increases, and the CCP imaging includes spurious streaking at multiple depths, rendering the Moho converter unclear.

We observed two regionally extensive midcrustal converters in the CCP profiles (Fig. 7), one visible in the northern portions of the CCP sections, and the second appearing in the southern portions of the generally N-S–trending sections. The southern converter dips southward from ~12 km depth at 46.5°S to 17 km at ~47.6°S. The northern converter dips northward from 12 to 13 km depth at 46.5°S to ~20 km at ~44.5°S. Assuming the converters form a continuous surface at midcrustal depths, we can show that this surface culminates at depths of ~15 km along a linear, approximately east-west–striking zone between ~46.25°S and 46.5°S.

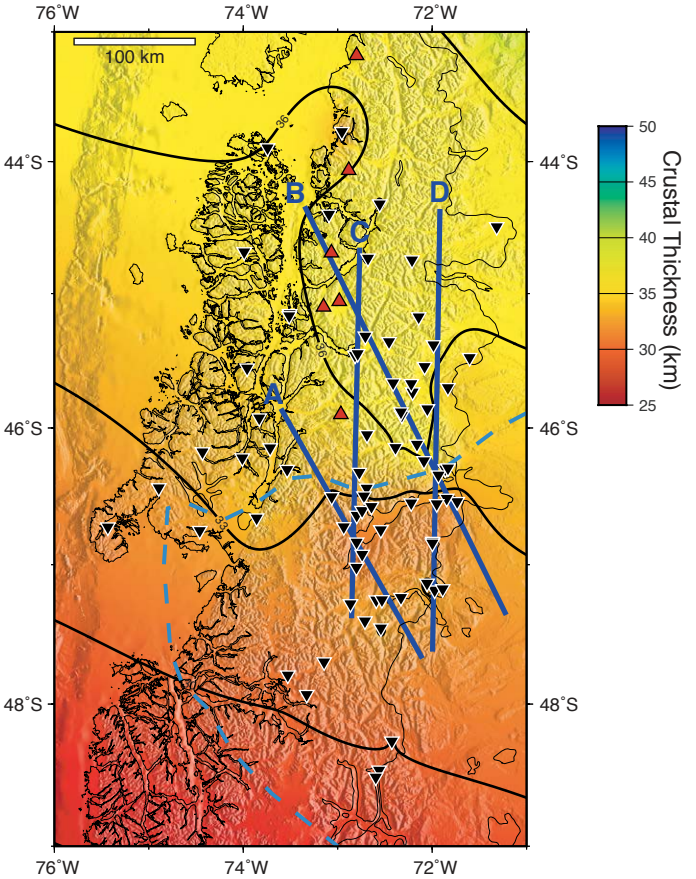

Figure 6. Common conversion point (CCP) stacking results: crustal thickness values. Dark blue lines show locations of cross sections of the CCP volume shown in Figure 7. Blue dashed line marks the edge of the slab window at 50 km depth from Russo et al. (2010a).

DISCUSSION

H-k Stacking

Our results at a group of eastern stations (~72°W), from both the CRSP and SEARCH deployments, exhibited bands of *H* and *k* values that fit the bootstrapped receiver function data equally well (Fig. 4; see also Figs. S9–S16 [footnote 1]). The *H-k* results for this region showed a clear and sudden south-to-north decrease in apparent crustal thickness from ~41–42 km at 46.5°S to ~30–32 km at 45.5°S at ~72°W (Fig. 5A). This region also coincides with an area of high variability in *k* values, from ~1.7 to ~1.8, with no corresponding changes in surface geology (Fig. 5B). We showed above (see *H-k* Results) that these ambiguities in the *H-k* grid search results at these eastern stations can be ameliorated by binning of the receiver functions into groups from northerly and southerly back azimuths and rerunning the grid search. Crustal thicknesses from these rebinned results are consistent with a strong, short-wavelength variation in crustal structure: *H* values from southern back-azimuth receiver functions were 33–47 km, but those for northern back-azimuth receiver functions were only 25–33 km. The Moho beneath the Eastern metamorphic complex and the Patagonia Ranges deepens by ~12 km over a N-S distance less than 50 km, indicating a northward Moho dip of ~11°, assuming the change in Moho depth is linear. The *H-k* grid search method is best suited for mode conversions that occur at sharp, laterally continuous horizontal interfaces (e.g., Ammon, 1991; Cassidy, 1992). Thus, given evidence that this assumption is violated in the eastern study area, the *H-k* Moho depth picks may not be accurate estimates of the crustal thickness in this region. Therefore, for the group of stations east of ~73°W, we derived our interpretations from the CCP stacking results. For the more widely separated stations of the

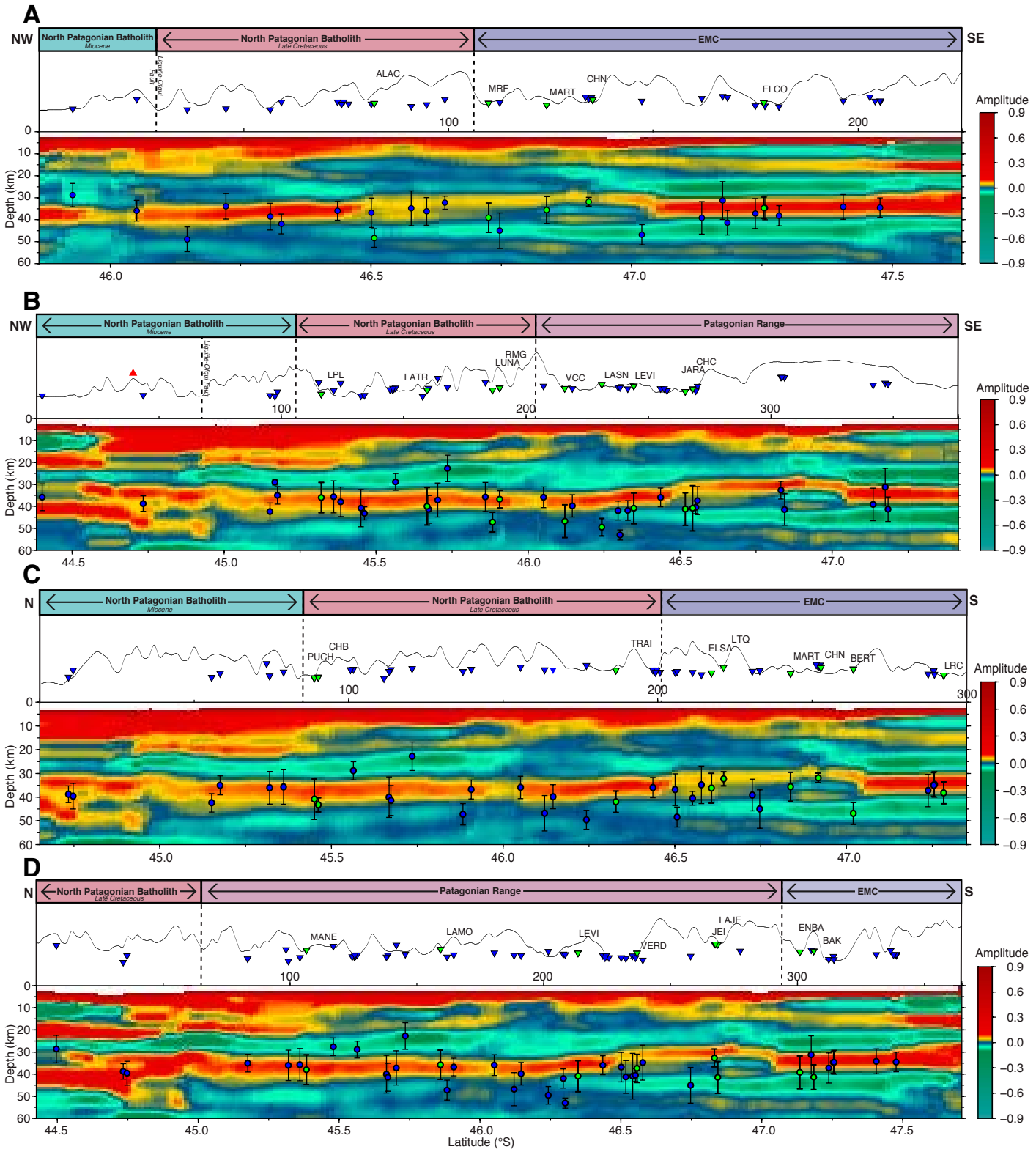

Figure 7. Common conversion point (CCP) stacking profiles (see Fig. 6 for section line locations). Overlain on the profiles in blue and green points are the corresponding *H-k* stacking results for each station; error bars show standard deviations in depth. Plotted above the CCP profiles are the geologic units and topography of the profile with a vertical exaggeration of 10×. Inverted green triangles show station locations along the profile; blue inverted triangles represent stations with 0.5° of the profile. EMC—Eastern metamorphic complex.

Taitao Peninsula and Chonos and Guaitecas islands, the *H-k* stacking results showed more easily identifiable Moho conversions (Figs. S1–S4) and a single major band in the *H-k* stacking (Figs. S9–S12), which are robust, and the following discussion of crustal thicknesses in those areas was derived from the *H-k* stacking results (Fig. 8).

We interpret crustal thickness differences between the Taitao Peninsula and the northern Chonos and Guaitecas Archipelago islands to be the result of subduction erosion and crustal thinning due to the subduction of the Chile Ridge beneath Taitao during the last 6 m.y. The crust of overriding South America beneath the southern Taitao Peninsula has been thinned to 28–34 km, whereas crustal thickness is systematically greater, 35–55 km, where the Chile Ridge has not yet subducted, beneath northern Taitao and the Chonos Archipelago. The young oceanic lithosphere of the Chile Ridge is relatively hot and consequently relatively buoyant. The increased buoyancy results in greater subduction erosion and thinning of the overriding South American crust as the ridge subducts (Bourgois et al., 1996).

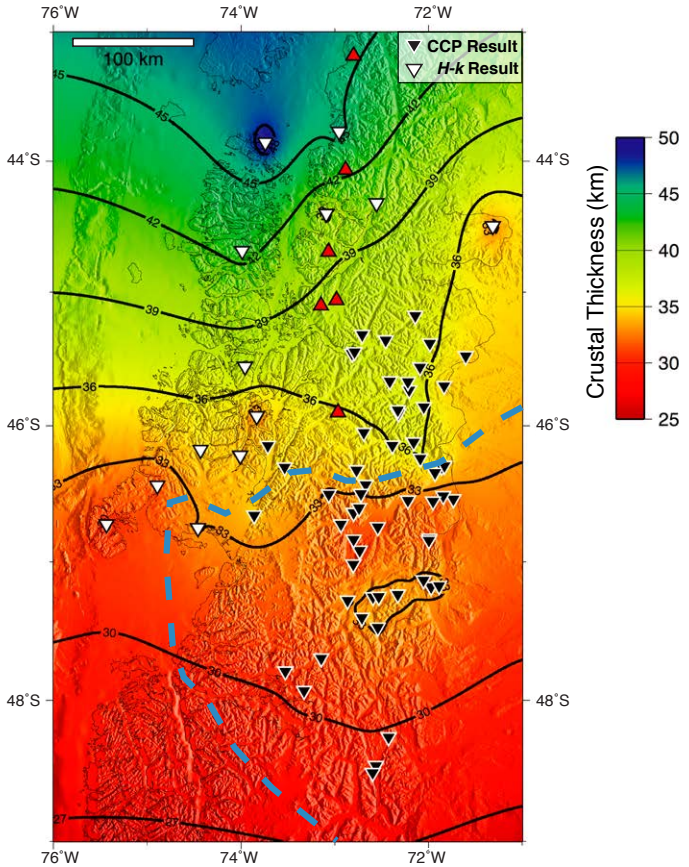

Figure 8. Combined crustal thickness map. Black-filled inverted triangles are stations for which crustal thickness estimates were derived from the common conversion point (CCP) stacking method, and white inverted triangles are stations with *H-k* crustal thickness estimates. Blue dashed line marks the edge of the slab window at 50 km depth from Russo et al. (2010a).

The three stations situated on the southern Taitao Peninsula have *k* values of ~1.64, in strong contrast to the ~1.82 values of the Western metamorphic complex in the Chonos islands, farther north. The ~1.82 values of the Western metamorphic complex are consistent with the values expected for the metaturbidites described by Hervé and Fanning (2001). The low *k* values found on the Taitao Peninsula may be associated with the granitic intrusions found on the peninsula (e.g., De Long et al., 1979). These intrusions are thought to be sourced from the partial melting of oceanic crust at the Chile Ridge, as it subducted (Kaeding et al., 1990; Kilian and Behrmann, 2003; Anma et al., 2009). Continental sediments forming the accretionary complex are also thought to have been incorporated into melts due to enhanced subduction erosion during ridge subduction (De Long et al., 1979).

In the region of the North Patagonian Batholith, crustal thickness attains values from 36 to 43 km, with generally thicker crust to the north but no apparent sharp transitions in Moho depth. The *k* values in this area vary from ~1.70 to ~1.77, a range that is consistent with a mean granitic crustal composition (Zandt and Ammon, 1995; Christensen, 1996), as expected given the observed composition of the North Patagonian Batholith.

CCP Stacking

The CCP stacking and *H-k* stacking methods yielded two different crustal structures for the region. The most significant differences in crustal depth estimates were observed where the Moho derived from the CCP stacking method rapidly shallows from 35 to 30 km near 46.5°S and 47.0°S (Fig. 7). The discrepancies between the *H-k* and CCP results likely stem from the inappropriate assumptions inherent in the *H-k* method, which assumes velocities do not vary laterally beneath the station as converted waves pass through the Moho to the station. However, for a dipping or discontinuous Moho, incoming rays sample distinct portions of the Moho, which can produce discrepant depths of mode conversion, dependent on the ray's piercing point. The single Moho pick resulting from the *H-k* grid search in a region of varying conversion depths can then lead to spurious crustal thickness estimates (e.g., Fig. 4).

The CCP stack explicitly accounts for possible 3-D structure by combining receiver functions according to the common conversion point of ray paths beneath a group of stations, rather than stacking the ray paths at the stations themselves. The presence of the high-amplitude midcrustal converters illuminated by the CCP results provides the key for understanding the *H-k* results: The shallow Moho depths picked by the *H-k* grid search, north of 45.5°S in the back-arc region (Figs. 6 and 7), appear to have been influenced by the presence

of these midcrustal converters. However, the actual Moho is visible in the CCP stack imaging beneath these midcrustal converting interfaces. Thus, the CCP stack results provide a more reliable estimate of crustal structure and were used for interpretations of the back-arc crustal structure, wherever possible.

Midcrustal Converters

The midcrustal converters we resolved in the data strike approximately east-west, culminating between ~46.25°S and 46.5°S from depths of 15 km at ~47.3°S and 21 km at ~44.5°S (Fig. 9). In order to produce a P-to-S conversion, the generative interfaces must entail a reasonably strong impedance contrast. Therefore, juxtaposition of rocks of distinct seismic velocity and/or density, or of strongly varying seismic anisotropy, or perhaps of varying physical state, i.e., partial melt, may be possible sources of these conversions. The observed midcrustal converters may represent transitions in lithology, juxtaposing rocks of different densities; they may be décollement or ductile fault surfaces characterized by strong petrologic fabrics and therefore strong seismic anisotropy; and at least in some places, they may be areas of partial melt underlying the active Southern volcanic zone (e.g., Wittlinger et al., 2004; Gans et al., 2011; Shi et al., 2015; Stanciu et al., 2016). The midcrustal converters are not uniquely spatially associated with the North Patagonian Batholith rocks, so conversions generated by a current midcrustal accumulation of partial melt seems unlikely. If a converter is a highly anisotropic midcrustal décollement, this surface is very extensive regionally, and would require strong shearing displacement along thousands of square kilometers without any apparent surface manifestation of such shear. We note, also, that the converters apparently underlie fairly heterogeneous geology, including the active arc, in part, and thus an ancient origin for the surface seems improbable.

Thus, the most likely origin of the midcrustal converters is a juxtaposition of different upper- and lower-crustal lithologies. The regional geology is consistent with a felsic mean composition of the upper crust. Several lines of evidence point to a more mafic lower crust underlying the study area, generally. Petrologic studies on the widespread Jurassic rhyolitic rocks of Patagonia,

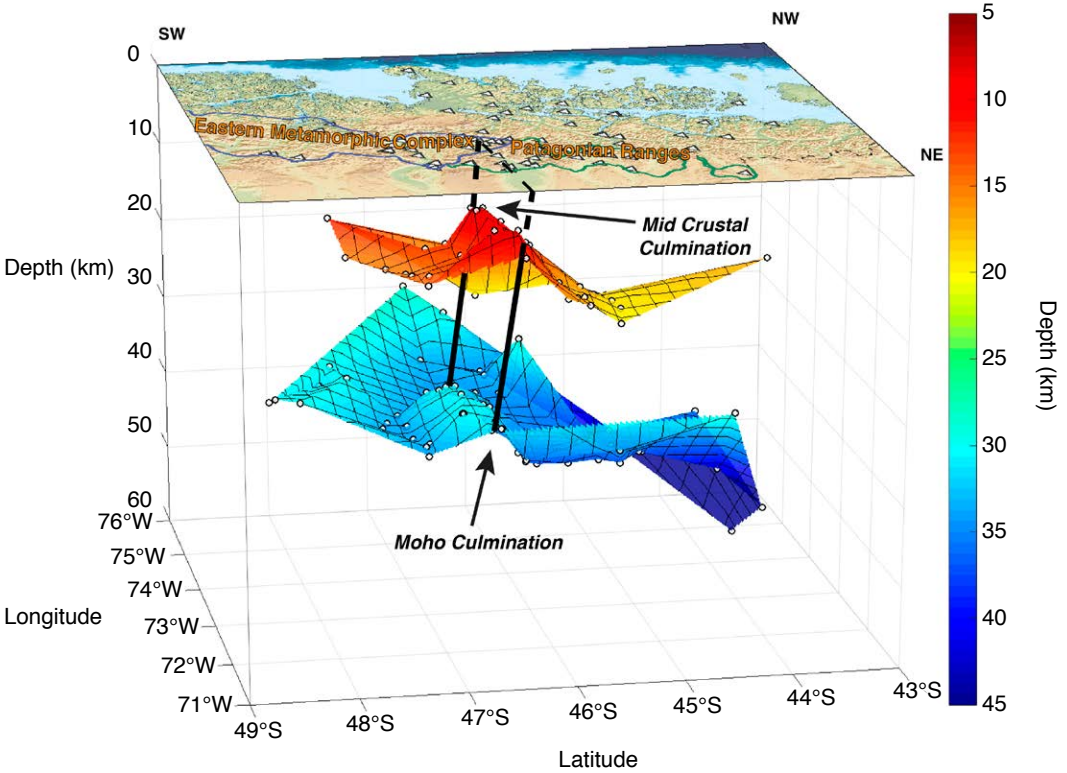

Figure 9. Three-dimensional (3-D) crustal structure showing the surfaces of the midcrustal converter and Moho projected beneath stations from *H-k* and common conversion point (CCP) results. White spheres show station locations projected onto the converter and Moho surfaces. Vertical exaggeration: ~10.7.

including those of the Patagonian Ranges, which outcrop above the northern midcrustal converter, have shown that these felsic rocks likely stem from Jurassic partial melting of late Proterozoic mafic lower-crust units (Pankhurst and Rapela, 1995; Pankhurst et al., 2000). The northern midcrustal converter may therefore be the interface between this felsic upper crust and Grenvillian-aged mafic basement.

The midcrustal converter to the south may similarly represent an interface between a mafic lower and felsic upper crust. The southern midcrustal converter overlies a region of thinner crust that we have identified as the northernmost crust of the Austral Basin. The Austral Basin opened as the result of regional extension during the Jurassic (Varela et al., 2012) and developed into a back-arc basin, the Rocas Verdes Basin, south of our study area during the Early Cretaceous (Dalziel, 1974; Wilson, 1991). The southern midcrustal converter may represent the top surface of mafic lower crust that formed during this extension. Alternatively, this crust could also comprise felsic upper crust over a Grenville-age, or even older (see Schilling et al., 2017), mafic lower crust, as we postulated for the crust farther north. We note that such heterogeneous crust was formed ubiquitously in collisional settings around the Gondwana perimeter (Foster and Goscombe, 2013), including, apparently, in Patagonia.

Crustal Thicknesses and Architecture

Results from the CCP stacking method delimit crustal thicknesses between 30 and 38 km in the arc and back-arc regions (Figs. 6 and 7). The Moho smoothly varies from ~37 km depth at the on-land northern margin of our study area at ~45°S, shallowing southward. A sharp jump in the Moho, from 35 km to ~30 km depth, occurs at 46.5°S. The Moho depth remains constant southward to 47°S, where it deepens again to 35 km and then smoothly shallows to 32–33 km at ~47.5°S.

Changes in depth of the Moho are not obviously associated with the surface geology, particularly where the voluminous Patagonian batholiths mask evidence of crustal deformation, except for perhaps the east-west–trending shallowing of the Moho at 46.5°S–47.0°S (Fig. 7). This Moho culmination (Figs. 8 and 9) coincides with the abrupt change at the surface from outcrops of the Patagonian Range to the north along the Chile-Argentina border to those of the Eastern metamorphic complex farther south (Fig. 9). The Moho culmination also coincides spatially with the approximately east-west–trending culmination of the midcrustal converter we described in the previous section (see Fig. 9). Finally, the midcrustal and Moho culminations lie immediately south of the northern boundary of the slab window (Figs. 7 and 9), as defined tomographically by Russo et al. (2010a). In the following discussion, we sought the simplest explanation for these spatial relationships (if any) among the Moho and midcrustal culminations, the slab window boundary, and the surface juxtaposition of the Paleozoic Eastern metamorphic complex and Mesozoic Patagonia Ranges outcrops. Any such relationship implies that these structures were likely cogenetic.

Five scenarios are viable to explain, at least in part, the along-strike change in crustal thickness and/or architecture beneath the eastern Andes: (1) The structure arose from juxtaposition of crustal blocks of different thickness during Paleozoic assembly of Patagonia; (2) the change in crustal structure entailed a south-dipping thrust formed during Paleozoic Patagonia assembly; (3) the change in crustal architecture is actually an extensional structure that formed during Mesozoic rifting of Gondwana; (4) crustal thinning south of ~46.5°S is due to late Cenozoic thermal erosion at the base of the lithosphere, caused by asthenospheric inflow into the slab window; or (5) crustal thinning south of ~46.5°S is a result of late Cenozoic mechanical erosion of the overriding plate due to subduction of the buoyant spreading ridge. We address each of these possibilities in the following paragraphs.

The late Cenozoic scenarios for producing the observed Moho and midcrustal culminations lying beneath the eastern Andes both involve ablation of the Patagonian mantle lithosphere from below, such that the lower crust was also affected. The observed crustal thinning manifests as a linear zone, trending east-west and occurring 150–200 km east of the subduction trench. This structure is thus well inboard from both the trench and the zone of interplate coupling; at these distances from the trench, any Nazca plate lithosphere generated at the Chile Ridge should have subducted to ~100–150 km depth. Furthermore, the slab window is well defined here (Russo et al., 2010a), and low seismic velocities extend into the transition zone from 50 km depth. Thus, although the crustal thinning we observed currently beneath the Taitao Peninsula, i.e., lying directly above very young, shallowly subducted Nazca plate lithosphere, can be explained by enhanced subduction erosion due to strong coupling between the subducting, thermally buoyant plate and the overriding forearc, such extensive removal (the Patagonian lithospheric mantle completely removed and the crust thinned by ~10 km) of the crust beneath the eastern Andes by mechanical coupling alone seems unlikely, given the presence of the slab window and the projected depth of any Nazca slab beneath the area of thinned crust.

Thermal erosion and basal removal of ~10 km of crust by late Cenozoic asthenospheric flow through the slab window (Russo et al., 2010a, 2010b) would also necessitate complete thermal ablation and removal of the subcrustal lithosphere beneath the eastern Andes. Such thermal ablation could explain the apparent relationship between the Moho and midcrustal culminations and the northern slab window edge (Fig. 7). The presence of extensive Miocene–Pleistocene "Meseta" basalts, which outcrop to the east of the Andes at the latitudes of the study region, and which are thought to have been caused by Chile Ridge subduction (e.g., Gorring et al., 1997; Gorring and Kay, 2001), is perhaps consistent with thermal ablation of the Patagonian mantle lithosphere and lower crust. However, exposures of older Paleozoic, more highly metamorphosed rocks of the Eastern metamorphic complex, relative to the Jurassic–Cretaceous, less metamorphosed Patagonian Ranges, imply differential crustal uplift south of the structural culminations and the slab window edge. It is not obvious that thermal ablation from below should result in uplift. Furthermore, removal of the Patagonian mantle lithosphere and some lower crust should reduce the strength of the thinned crustal remnant, which should then be weak relative to lithosphere to the north that has not experienced such

ablation. Given enhanced interplate coupling due to subduction of the Chile Ridge—while ablation is occurring—we would expect such thinned, weak Patagonian crust to undergo stronger shortening in the convergence direction than that in areas immediately to the north that were not affected by ridge subduction and slab window formation. However, strongly developed compressional deformation in the southern Andes is not observed, and in fact, Schilling et al. (2017, see their figure 7) showed that the Patagonian lithosphere here is relatively thick, i.e., intact and not significantly thinned, implying it is relatively strong. Thus, we regard this scenario as less likely.

Could the observed crustal architecture be the result of Mesozoic rifting, as Gondwana separated into the current southern continent group? The thinner Patagonian crust south of the Moho and midcrustal culminations is a point in favor of this idea. If so, the implication is that this crust was thicker, but then it thinned during widespread Mesozoic rifting (e.g., Varela et al., 2012). The elevation of the Moho as the crust thins, as per the Moho culmination, is also potentially consistent with a rifting origin for the observed crustal architecture. Note, first, that the Moho and midcrustal culminations are not aligned vertically: The Moho culmination apparently lies south of the midcrustal culmination, and both structures strike apparently east-west. Thus, if these structural offsets are parts of a rifting structure or complex of structures (a large-scale fault, or fault zone, for example), that structure dips ~20° to the south (Fig. 9). The position of the Moho and midcrustal culminations, at approximately the northern end of the Austral Basin (Fig. 1), and the current approximately east-west strike and southerly dip of the putative rifting structure imply opening of the basin due to approximately north-south extensional stresses in this area, although the rifting generally seems to have opened linear basins with a more NW-SE trend, generally, farther to the south. A significant point against a rifting origin for this crustal architecture is that the southward dip of the potential rifting structure implies that it underlies the Eastern metamorphic complex (Fig. 9). If, as we implied above, this structure juxtaposes the Eastern metamorphic complex and the Patagonian Ranges at depth, then it places the older, Paleozoic Eastern metamorphic complex apparently above the younger Jurassic–Cretaceous rocks of the Patagonian Ranges, i.e., a thrust geometry, not obviously consistent with a rifting origin. We can retain the hypothesis that the crustal architecture here is due to rifting if we dispense with the idea that the structure is also the surface along which the Eastern metamorphic complex and Patagonian Ranges are juxtaposed. The nature of the actual boundary between the two major outcropping units of the eastern Andes in the study area is then unresolved.

What of our two remaining possibilities, i.e., that the crustal architecture here is due to juxtaposition of terranes with different crustal thicknesses during Paleozoic amalgamation to form the composite Patagonian terrane, or the observed crustal structure was actually formed during the assembly of Patagonia? The hypothesis that the structure is a thrust fault that was active during Paleozoic assembly of Patagonia is viable if we dispense with the notion that this structure also juxtaposes the Eastern metamorphic complex and the Patagonian Ranges, since the latter developed only during the Mesozoic. The observed crustal architecture obviously could have developed by thrusting of a thin Deseado Massif terrane over a thicker North Patagonia/Somún Cura terrane during Paleozoic assembly of Patagonia (e.g., Ramos, 2008; Mundl et al., 2015; Schilling et al., 2017). Thus, the east-west–trending Moho culmination marking pronounced crustal thinning at 46.5°S–47.0°S (Fig. 9) almost certainly reflects crustal thickness differences that predate eastward subduction of Pacific Basin oceanic lithosphere beneath South America. We note that the metamorphism of the Eastern metamorphic complex was attributed by Bell and Suárez (2000) to Patagonian microplate assembly processes. The thinner crust in the southeasternmost portion of our study area lies within the northwestern portion of the Austral Basin (Ramos, 2008) and is likely the Paleoproterozoic Deseado Massif. Thicker crust to the north along and east of the Andes is likely the North Patagonian Batholith/Somún Cura terrane.

CONCLUSIONS

We used the *H-k* and CCP stacking methods on teleseismic receiver functions recorded at stations inboard of and across the subducting Chile Ridge in order to study crustal thickness and structures of the overriding South America plate. The results of the *H-k* and CCP methods were consistent for most of the region; however, in the eastern portion of the study region, both CCP images and *H-k* results deriving from azimuthally binned receiver function stacks revealed strong, short-length-scale differences in Moho depth, with as much as a 12 km difference between the crustal thickness estimates from the two techniques. The differences between crustal thickness observations are attributed to the assumptions made by the *H-k* stacking method. The results of the CCP stacking method, which accounted for these assumptions, thereby supersede the *H-k* stacking method results for interpretations. However, use of the CCP method throughout the region was limited spatially due to heterogeneous station distributions.

The results from both methods were combined in order to create a comprehensive crustal thickness map of the region. From the *H-k* stacking method, the direct effect of the subducting ridge on South America can be seen in crustal thickness differences in forearc regions that have experienced ridge subduction, where the Moho depth is 28–35 km. This contrasts with stations to the north of the Chile triple junction that have not experienced ridge subduction, which have crustal thicknesses of 34–45 km. Crustal thinning above the current ridge subduction is a result of enhanced subduction erosion due to the Chile Ridge's greater buoyancy. The South American forearc crust above the subducted Nazca plate is as much as 28 km thicker than forearc crust recently affected by ridge subduction and is as much as 11 km thicker than forearc crust above the subducting Antarctic plate.

From the CCP results, the regional Moho, overall, dips northward from 32–33 km at the southern margin of our study region at ~47.6°S to 37–38 km at the northern margin at ~45.0°S. At 47.0°S, the smoothly varying Moho is disrupted by a sharp shallowing in depth from 35 to 30 km, where the depth of the Moho northward remains constant to 46.5°S. At 46.5°S, the Moho deepens

again to 35 km and continues to deepen to 37–38 km at 45.0°S. The east-west trend of the thinned crust between 46.5°S and 47°S and its distance from the subduction zone implies that it is likely a primary structure of the crust related to the assembly of Patagonia. The observed crustal architecture is consistent with thrusting of a thin Deseado Massif terrane over a thicker North Patagonia/Somún Cura terrane during Paleozoic assembly of Patagonia.

ACKNOWLEDGMENTS

We are very grateful to Diana Comte, Victor Mocanu, Ruth Murdie, Alejandro Gallego, Eduardo Moscoso, and John VanDecar, whose strenuous efforts ensured the success of the Chile Ridge Subduction Project. Likewise, we thank Matt Miller, Klaus Bataille, and Keith Priestly for their efforts in deploying and maintaining the SEARCH network, and for allowing use of the data collected. This work would not have been possible without the help of the following people: Umberto Fuenzalida, Hernan Marilao, and Carmen Gloria of the Universidad de Chile; Juan Fica, Claudio Manzur, Carlos Llautureo, Corporacion Nacional Forestal de Chile (CONAF); Monica Retamal Maturana, Banco Estado; Carabineros de Chile del Region de Aysen; Armada de Chile; Comandante Roldan, Major Wellkner, Cuerpo Militar de Trabajo del Ejercito de Chile; Luis Miranda Chiguay, Alcaldes de Aysen, Melinka, Rio Ibanez, Lago Verde; Ejercito de Chile; Carlos Feliu Ruiz, Aeronautica de Chile; Don Luis Hidalgo, Automotriz Varona; Don Gustavo Lopez y Hostal Bon; Mike Fort, Noel Barstow, Bruce Beaudoin, Jim Fowler of IRIS PASSCAL; Juan Gallardo, Axel Hernandez, Hernan Aguilar, Jose Geicha Nauto, Tripulacion de LM Petrel IV CONAF; Gilles Rigaud, Aurelia Rigaud, Valerie Clouard, Lorena Palacio et Morgane; Eduardo Moscoso; Don Raul Hernandez, Fundo Los Nirres; Sergio Mirando Contreras Melinka; Victor Figueroa, Escuela Carlos Condell, Calete Andrade, Puerto Aguirre; Enrique Alcalde Cochrane; Luis Levin Bahia Murta; Baterias GAMI Puerto Montt; Mauricio Zambrano L., Coyhaique Centro de Llamadas; Rolando Burgos and Roselia Delgado, Fachinal; Aladin Jara, Gobernacion de Chile Chico; Rolando Toloza, Ministerio Obras Publicas; Mark and Señora Knipreth, Heart of the Andes Lodge; Heraldo Zapata Rivera, Ramon Villegas, Omar Tapia Vidal, Jorge Oyarzun Inostroza, Tripulacion de El Aleph; Sandalio Munoz, Fundo La Pedregosa; Don Cristian Brautigam; and the many, many people of Region XI, Aysen, who helped us enthusiastically and unstintingly and without whom this work would have been impossible. We are grateful to C. Ammon and L. Zhu for use of their receiver function and *H-k* grid search codes and A. Christian Stanciu for advice on using these codes. Seismic instruments deployed as part of the Chile Ridge Subduction Project were provided by the Incorporated Research Institutions for Seismology (IRIS) through the PASSCAL Instrument Center at New Mexico Tech. Data collected are available through the IRIS Data Management Center. The facilities of the IRIS Consortium are supported by the National Science Foundation under cooperative agreement EAR-1261681 and the U.S. Department of Energy National Nuclear Security Administration. This work was supported by U.S. National Science Foundation grant EAR-0126244 and Comisión Nacional de Investigación Científica y Tecnológica (CONICYT) Chile grant 1050367.

REFERENCES CITED

Ammon, C.J., 1991, The isolation of receiver effects from teleseismic P waveforms: Bulletin of the Seismological Society of America, v. 81, p. 2504–2510.

Ammon, C.J., Randall, G.E., and Zandt, G., 1990, On the nonuniqueness of receiver function inversions: Journal of Geophysical Research, v. 95, p. 15303–15318, https://doi.org/10.1029/JB095iB10p15303.

Anma, R., Armstrong, R., Orihashi, Y., Ike, S.I., Shin, K.C., Kon, Y., Komiya, T., Ota, T., Kagashima, S.I., Shibuya, T., and Yamamoto, S., 2009, Are the Taitao granites formed due to subduction of the Chile Ridge?: Lithos, v. 1131, p. 246–258, https://doi.org/10.1016/j.lithos.2009.05.018.

Bell, C.M., and Suárez, M., 2000, The Rıo Lácteo Formation of southern Chile. Late Paleozoic orogeny in the Andes of southernmost South America: Journal of South American Earth Sciences, v. 13, p. 133–145, https://doi.org/10.1016/S0895-9811(00)00005-5.

Bishop, B.T., Beck, S.L., Zandt, G., Wagner, L., Long, M., Antonijevic, S.K., Kumar, A., and Tavera, H., 2017, Causes and consequences of flat-slab subduction in southern Peru: Geosphere, v. 13, no. 5, p. 1392–1407, https://doi.org/10.1130/GES01440.1.

Bourgois, J., Martin, H., Lagabrielle, Y., Le Moigne, J., and Frutos Jara, J., 1996, Subduction erosion related to spreading-ridge subduction: Taitao Peninsula, Chile margin triple junction area: Geology, v. 24, p. 723–726, https://doi.org/10.1130/0091-7613(1996)024<0723:SERTSR>2.3.CO;2.

Bourgois, J., Lagabrielle, Y., Martin, H., Dyment, J., Frutos, J. and Cisternas, M.E., 2016, A review on forearc ophiolite obduction, adakite-like generation, and slab window development at the Chile triple junction area: uniformitarian framework for spreading-ridge subduction. Pure and Applied Geophysics, v. 173, p. 3217–3246, https://doi.org/10.1007/s00024-016-1317-9.

Breitsprecher, K., and Thorkelson, D.J., 2009, Neogene kinematic history of Nazca-Antarctic-Phoenix slab windows beneath Patagonia and the Antarctic Peninsula: Tectonophysics, v. 464, p. 10–20, https://doi.org/10.1016/j.tecto.2008.02.013.

Cande, S.C., and Leslie, R.B., 1986, Late Cenozoic tectonics of the southern Chile Trench: Journal of Geophysical Research, v. 91, p. 471–496, https://doi.org/10.1029/JB091iB01p00471.

Cassidy, J.F., 1992, Numerical experiments in broadband receiver functions analysis: Bulletin of the Seismological Society of America, v. 82–83, p. 1453–1474.

Christensen, N.I., 1996, Poisson's ratio and crustal seismology: Journal of Geophysical Research, v. 101, p. 3139–3156, https://doi.org/10.1029/95JB03446.

Clarke, T.J., and Silver, P.G., 1993, Estimation of crustal Poisson's ratio from broad band teleseismic data: Geophysical Research Letters, v. 20, p. 241–244, https://doi.org/10.1029/92GL02922.

Dalziel, I.W.D., 1974, Evolution of the margins of the Scotia Sea, *in* Burk, C.A., and Drake, C.L., eds., The Geology of Continental Margins: Berlin, Springer, p. 567–579.

De La Cruz, R., Suárez, M., Morata, D., Espinoza, F., and Troncoso, A., 2003, El Cenozoico del Lago General Carrera, Aysén, Chile 46°30′–47°15′S: Estratigrafía y tectónica: Presented at Congreso Geológico Chileno 10, Concepción, Chile, 6–10 October.

DeLong, S., Schwartz, W., and Anderson, R., 1979, Thermal effects of ridge subduction: Earth and Planetary Science Letters, v. 44, p. 239–246, https://doi.org/10.1016/0012-821X(79)90172-9.

Dueker, K.G., and Sheehan, A.F., 1997, Mantle discontinuity structure from midpoint stacks of converted P to S waves across the Yellowstone hotspot track: Journal of Geophysical Research, v. 102, p. 8313–8327, https://doi.org/10.1029/96JB03857.

Foster, D.A., and Goscombe, B.D., 2013, Continental growth and recycling in convergent orogens with large turbidite fans on oceanic crust: Geosciences, v. 3, p. 354–388, https://doi.org/10.3390/geosciences3030354.

Gans, C.R., Beck, S.L., Zandt, G., Gilbert, H., Alvarado, P., Anderson, M., and Linkimer, L., 2011, Continental and oceanic crustal structure of the Pampean flat slab region, western Argentina, using receiver function analysis: New high-resolution results: Geophysical Journal International, v. 186, p. 45–58, https://doi.org/10.1111/j.1365-246X.2011.05023.x.

Gorring, M.L., and Kay, S.M., 2001, Mantle processes and sources of Neogene slab window magmas from southern Patagonia, Argentina: Journal of Petrology, v. 42, p. 1067–1094, https://doi.org/10.1093/petrology/42.6.1067.

Gorring, M.L., Kay, S.M., Zeitler, P.K., Ramos, V.A., Rubiolo, D., Fernandez, M.I., and Panza, J.L., 1997, Neogene Patagonian plateau lavas: Continental magmas associated with ridge collision at the Chile triple junction: Tectonics, v. 16, p. 1–17, https://doi.org/10.1029/96TC03368.

Herron, E.M., Cande, S.C., and Hall, B.R., 1981, An active spreading center collides with a subduction zone: A geophysical survey of the Chile margin triple junction, *in* Kulm, L.D., Dymond, J., Dasch, E.J., Hussong, D.M., and Roderick, R., eds., Nazca Plate: Crustal Formation and Andean Convergence: Geological Society of America Memoir 154, p. 683–702, https://doi.org/10.1130/MEM154-p683.

Hervé, F., and Fanning, C.M., 2001, Late Triassic detrital zircons in meta-turbidites of the Chonos metamorphic complex, southern Chile: Revista Geológica de Chile, v. 281, p. 91–104, https://doi.org/10.4067/S0716-02082001000100005.

Hervé, F., Fanning, C.M., and Pankhurst, R.J., 2003, Detrital zircon age patterns and provenance of the metamorphic complexes of southern Chile: Journal of South American Earth Sciences, v. 16, p. 107–123, https://doi.org/10.1016/S0895-9811(03)00022-1.

Kaeding, M., Forsythe, R., and Nelson, E., 1990, Geochemistry of the Taitao ophiolite and near-trench intrusions from the Chile margin triple junction: Journal of South American Earth Sciences, v. 3, p. 161–177, https://doi.org/10.1016/0895-9811(90)90001-H.

Kennett, B.L.N., and Engdahl, E.R., 1991, Traveltimes for global earthquake location and phase identification: Geophysical Journal International, v. 105, p. 429–465, https://doi.org/10.1111/j.1365-246X.1991.tb06724.x.

Kilian, R., and Behrmann, J.H., 2003, Geochemical constraints on the sources of southern Chile Trench sediments and their recycling in arc magmas of the Southern Andes: Journal of the Geological Society [London], v. 160, p. 57–70, https://doi.org/10.1144/0016-764901-143.

Lagabrielle, Y., Suarez, M., Malavieille, J., Morata, D., Espinoza, F., Maury, R.C., Scalabrino, B., Barbero, L., Cruz, R.D.L., Rossello, E., and Bellon, H., 2007, Pliocene extensional tectonics in the eastern Central Patagonian Cordillera: Geochronological constraints and new field evidence: Terra Nova, v. 19, p. 413–424, https://doi.org/10.1111/j.1365-3121.2007.00766.x.

Langston, C.A., 1977, Corvallis, Oregon, crustal and upper mantle structure from teleseismic P and S waves: Bulletin of the Seismological Society of America, v. 67, p. 713–724.

Ligorria, J.P., and Ammon, C.J., 1999, Iterative deconvolution and receiver function estimation: Bulletin of the Seismological Society of America, v. 89, p. 1395–1400.

Morata, D., Espinoza, F., Polvé, M., Pelleter, E., Guivel, C., Lagabrielle, Y., Suarez, M., De La Cruz, R., Bellon, H., and Cotton, J., 2004, Asthenospheric-lithospheric interactions in Mio-Pliocene back-arc extensional magmatism in Patagonia: Tracing the window-slab geochemistry signature: Pucon, Chile, International Association of Volcanology and Chemistry of the Earth's Interior (IAVCEI) General Assembly, Abstract QE521.5.I58 2004.

Mundl, A., Ntaflos, T., Ackerman, L., Bizimis, M., Bjerg, E.A., and Hauzenberger, C.A., 2015, Mesoproterozoic and Paleoproterozoic subcontinental lithospheric mantle domains beneath southern Patagonia: Isotopic evidence for its connection to Africa and Antarctica: Geology, v. 43, p. 39–42, https://doi.org/10.1130/G36344.1.

Mundl, A., Ntaflos, T., Ackerman, L., Bizimis, M., Bjerg, E.A., Wegner, W., and Hauzenberger, C.A., 2016, Geochemical and Os-Hf-Sr isotopic characterization of North Patagonian mantle xenoliths: Implications for extensive melt extraction and percolation processes: Journal of Petrology, v. 57, p. 685–715, https://doi.org/10.1093/petrology/egv048.

Pankhurst, R.J., and Rapela, C.R., 1995, Production of Jurassic rhyolite by anatexis of the lower crust of Patagonia: Earth and Planetary Science Letters, v. 134, p. 23–36, https://doi.org/10.1016/0012-821X(95)00103-J.

Pankhurst, R.J., Leat, P.T., Sruoga, P., Rapela, C.W., Márquez, M., Storey, B.C., and Riley, T.R., 1998, The Chon Aike province of Patagonia and related rocks in West Antarctica: A silicic large igneous province: Journal of Volcanology and Geothermal Research, v. 81, p. 113–136, https://doi.org/10.1016/S0377-0273(97)00070-X.

Pankhurst, R.J., Weaver, S.D., Hervé, F., and Larrondo, P., 1999, Mesozoic–Cenozoic evolution of the North Patagonian Batholith in Aysen, southern Chile: Journal of the Geological Society [London], v. 156, p. 673–694, https://doi.org/10.1144/gsjgs.156.4.0673.

Pankhurst, R.J., Riley, T.R., Fanning, C.M., and Kelley, S.P., 2000, Episodic silicic volcanism in Patagonia and the Antarctic Peninsula: Chronology of magmatism associated with the break-up of Gondwana: Journal of Petrology, v. 41, p. 605–625, https://doi.org/10.1093/petrology/41.5.605.

Pankhurst, R.J., Rapela, C.W., Fanning, C.M., and Márquez, M., 2006, Gondwanide continental collision and the origin of Patagonia: Earth-Science Reviews, v. 76, p. 235–257, https://doi.org/10.1016/j.earscirev.2006.02.001.

Ramos, V.A., 1989, The birth of southern South America: American Scientist, v. 77, p. 444–450.

Ramos, V.A., 2008, Patagonia: A Paleozoic continent adrift?: Journal of South American Earth Sciences, v. 26, p. 235–251, https://doi.org/10.1016/j.jsames.2008.06.002.

Rapela, C.W., Pankhurst, R.J., Casquet, C., Fanning, C.M., Baldo, E.G., González-Casado, J.M., Galindo, C., and Dahlquist, J., 2007, The Río de la Plata craton and the assembly of SW Gondwana: Earth-Science Reviews, v. 83, p. 49–82, https://doi.org/10.1016/j.earscirev.2007.03.004.

Russo, R.M., VanDecar, J.C., Comte, D., Mocanu, V.I., Gallego, A., and Murdie, R.E., 2010a, Subduction of the Chile Ridge: Upper mantle structure and flow: GSA Today, v. 20, no. 9, p. 4–10, https://doi.org/10.1130/GSATG61A.1.

Russo, R.M., Gallego, A., Comte, D., Mocanu, V.I., Murdie, R.E., and VanDecar, J.C., 2010b, Source-side shear wave splitting and upper mantle flow in the Chile Ridge subduction region: Geology, v. 38, p. 707–710, https://doi.org/10.1130/G30920.1.

Sandvol, E., Seber, D., Calvert, A., and Barazangi, M., 1998, Grid search modeling of receiver functions: Implications for crustal structure in the Middle East and North Africa: Journal of Geophysical Research, v. 103, p. 26899–26917, https://doi.org/10.1029/98JB02238.

Schilling, M.E., Carlson, R.W., Tassara, A., Conceição, R.W., Bertotto, G.W., Vásquez, M., Muñoz, D., Jalowitzki, T., Gervasoni, F., and Morata, D., 2017, The origin of Patagonia revealed by Re-Os systematics of mantle xenoliths: Precambrian Research, v. 294, p. 15–32, https://doi.org/10.1016/j.precamres.2017.03.008.

Servicio Nacional de Geología y Minería (SERNAGEOMIN), 2003, Mapa Geológico de Chile: Versión Digital: Santiago, Chile, Servicio Nacional de Geología y Minería, Publicación Geológica Digital 4, CD-ROM, version 1.0, 2003.

Shi, D., Wu, Z., Klemperer, S.L., Zhao, W., Xue, G., and Su, H., 2015, Receiver function imaging of crustal suture, steep subduction, and mantle wedge in the eastern India–Tibet continental collision zone: Earth and Planetary Science Letters, v. 414, p. 6–15, https://doi.org/10.1016/j.epsl.2014.12.055.

Stanciu, A.C., Russo, R.M., Mocanu, V.I., Bremner, P.M., Hongsresawat, S., Torpey, M.E., VanDecar, J.C., Foster, D.A., and Hole, J.A., 2016, Crustal structure beneath the Blue Mountains terranes and cratonic North America, eastern Oregon and Idaho, from teleseismic receiver functions: Journal of Geophysical Research–Solid Earth, v. 121, p. 5049–5067, https://doi.org/10.1002/2016JB012989.

Varela, A.N., Poiré, D.G., Martin, T., Gerdes, A., Goin, F.J., Gelfo, J.N., and Hoffmann, S., 2012, U-Pb zircon constraints on the age of the Cretaceous Mata Amarilla Formation, southern Patagonia, Argentina: Its relationship with the evolution of the Austral Basin: Andean Geology, v. 393, p. 359–379, https://doi.org/10.5027/andgeoV39n3-a01.

Wang, K., Hu, Y., Bevis, M., Kendrick, E., Smalley, R., Vargas, R.B., and Lauría, E., 2007, Crustal motion in the zone of the 1960 Chile earthquake: Detangling earthquake-cycle deformation and forearc-sliver translation: Geochemistry Geophysics Geosystems, v. 8, no. 10, Q10010, https://doi.org/10.1029/2007GC001721.

Wilson, T.J., 1991, Transition from back-arc to foreland basin development in the southernmost Andes: Stratigraphic record from the Ultima Esperanza District, Chile: Geological Society of America Bulletin, v. 103, p. 98–111, https://doi.org/10.1130/0016-7606(1991)103<0098:TFBATF>2.3.CO;2.

Wittlinger, G., Vergne, J., Tapponnier, P., Farra, V., Poupinet, G., Jiang, M., Su, H., Herquel, G., and Paul, A., 2004, Teleseismic imaging of subducting lithosphere and Moho offsets beneath western Tibet: Earth and Planetary Science Letters, v. 221, p. 117–130, https://doi.org/10.1016/S0012-821X(03)00723-4.

Zandt, G., and Ammon, C.J., 1995, Continental crust composition constrained by measurements of crustal Poisson's ratio: Letters to Nature, v. 374, p. 152–154, https://doi.org/10.1038/374152a0.

Zhu, L., and Kanamori, H., 2000, Moho depth variation in southern California from teleseismic receiver functions: Journal of Geophysical Research, v. 105, p. 2969–2980, https://doi.org/10.1029/1999JB900322.

Zhu, L., Mitchell, B.J., Akyol, N., Cemen, I., and Kekovali, K., 2006, Crustal thickness variations in the Aegean region and implications for the extension of continental crust: Journal of Geophysical Research–Solid Earth, v. 111, no. B1, B01301, https://doi.org/10.1029/2005JB00377.